Valence-Shell Photoionization of C 4 H 5 : The 2-Butyn-1-yl Radical

H. Hrodmarsson, J.-C. Loison, U. Jacovella, D. M. P. Holland, S. Boyé-Péronne, B. Gans, G. Garcia, L. Nahon, S. Pratt

Valence-Shell Photoionization of C_4H_5: the 2-Butyn-1-yl Radical

H. R. Hrodmarsson,[a] J.-C. Loison,[b] U. Jacovella,[c†] D. M. P. Holland,[d] S. Boyé-Péronne,[e] B. Gans,[e] G. A. Garcia,[a] L. Nahon,[a] and S. T. Pratt[f*]

[a]Synchrotron Soleil, L'Orme des Merisiers, F-91192 Gif-sur-Yvette, France

[b]Institut des Sciences Moléculaires, Université Bordeaux, Talence, France

[c]Laboratorium für Physikalische Chemie, ETH Zürich, 8093 Zürich, Switzerland

[d]STFC, Daresbury Laboratory, Daresbury, Warrington, Cheshire WA4 4AD, UK

[e]Institut des Sciences Moléculaires d'Orsay, UMR 8214, CNRS & Univ. Paris-Sud & Université Paris-Saclay, F-91405 Orsay, France

[f]Chemical Sciences and Engineering Division, Argonne National Laboratory, Argonne, IL 60439 USA

[†]Current address: University of Melbourne, School of Chemistry, Masson Rd, Parkville VIC 3052, Australia
*Corresponding Author, email: stpratt@anl.gov

ABSTRACT

We present new high-resolution data on the photoionization of the 2-butyn-1-yl radical ($CH_3C{\equiv}C\text{-}{\bullet}CH_2$) formed by H-atom abstraction from 2-butyne by F atoms. The spectra were recorded from 7.7 to 11 eV by using double-imaging, photoelectron-photoion coincidence spectroscopy, which allows the unambiguous correlation of photoelectron data and the mass of the species. The photoionization spectrum shows significant resonant autoionizing structure converging to excited states of the $C_4H_5^+$ cation, similar to what is observed in the closely related propargyl radical ($HC{\equiv}C\text{-}{\bullet}CH_2$). The threshold photoelectron spectrum, obtained with a resolution of 17 meV, is also reported. This spectrum is consistent with previous measurements of the first photoionization band, but has been extended to higher energy to allow the observation of bands corresponding to excited electronic states of the ion. A refined value of the adiabatic ionization energy is extracted: $IE(C_4H_5) = 7.93 \pm 0.01$ eV. A determination of the absolute photoionization cross section of the 2-butyn-1-yl radical at 9.7 eV is also reported: $\sigma_{ion}(C_4H_5) = 6.1 \pm 1.8$ Mb.

I. INTRODUCTION

Small hydrocarbon radicals play an important role in the gas-phase chemistry of many reacting systems, including combustion,[1,2] low-temperature plasmas,[3] and planetary atmospheres.[4] Over the last decade, photoionization mass spectrometry coupled to a tunable light source has proven to be a powerful tool for characterizing radicals and their reactions in complex environments.[5-9] The technique is applicable to any molecule, and the selectivity of the detection allows the identification of species with different masses, while the wavelength dependence of the ionization signal provides a means to distinguish, in favorable cases, among multiple isomers at a given mass. The utility of this approach can be further enhanced by a knowledge of the relevant absolute photoionization cross sections,[10] which, when coupled with a knowledge of the photon flux and the geometry of the interaction region, can provide a determination of the species' concentrations. In this paper, we focus on the photoionization dynamics, photoelectron spectroscopy, and absolute photoionization cross section for the 2-butyn-1-yl, C_4H_5 radical. This radical is closely related to the important resonance-stabilized propargyl radical, C_3H_3, with the acetylenic H atom replaced by a methyl group.

Photoionization spectra typically show contributions both from direct ionization from the initial state into the energetically accessible continua, and from resonant autoionization features resulting from the decay of Rydberg states converging to higher lying states of the ion.[11,12] While the total energy of the autoionizing state is above the ionization threshold of the molecule, this energy is initially distributed amongst the electronic, vibrational, and rotational degrees of freedom of the molecule, and must be redistributed to provide one electron with sufficient energy to escape. The width of these resonances can span a wide range of values, reflecting the wide range of coupling strength among the relevant internal modes of the molecule.

In most molecules, the ionization energy is greater than the dissociation energy, so that, at least in principle, resonances that can autoionize can also predissociate. The photoionization spectrum

reflects this competition between decay processes through a loss in the expected intensity of the autoionizing resonance. In larger molecules, the resonances may also undergo fast radiationless transitions to neutral states with much lower principal quantum numbers and much greater vibrational energy. These states may ultimately dissociate or possibly fluoresce, but are unlikely to autoionize. As a result, the photoionization spectra of many larger molecules, as well as a significant number of smaller ones, often show very little resonant autoionization structure. Interestingly, the high-resolution photoionization spectrum of the propargyl radical shows considerable intense structure converging to electronically excited states of the $C_3H_3^+$ cation.[13-15] While the assignments of these resonances are currently tentative, their stability with respect to competing decay processes may be due to the relatively stiff structure of the radical, which could reduce the potential for radiationless transitions, or to the relative stability of the closed-shell propargyl $C_3H_3^+$ cation. The extent to which this resonance structure is preserved or modified in the more flexible radicals produced by the addition of a methyl rotor to the propargyl radical ($HC\equiv C\text{-}\bullet CH_2$), depending on which H atom is substituted, is thus of some interest. Two isomers of the butynyl radical are thus expected: the 2-butyn-1-yl radical ($CH_3C\equiv C\text{-}\bullet CH_2$) and the 1-butyn-3-yl ($HC\equiv C\text{-}\bullet CH\text{-}CH_3$) radical, and the structures of these radicals are shown in Figure 1.

The threshold photoelectron spectra (TPES) of the first band of both the 2-butyn-1-yl and 1-butyn-3-yl radicals have been reported previously by Lang *et al.*,[16] who created the radicals with a tubular pyrolysis source. Hansen *et al.*[17] have used photoionization mass spectrometry coupled to a low-pressure flame to characterize the chemistry of a number of different C_4H_3 and C_4H_5 radicals. Comparison of the experimental spectra with theoretical calculations of ionization thresholds and Franck-Condon envelopes helped them identify which isomers were present. Photoionization mass spectrometry has also been used by Chin *et al.*[18] to identify C_4H_5 radicals formed in crossed molecular beam studies of the C + C_3H_6 reaction. Unfortunately for our purposes, the spectral resolution of the previous photoionization spectra was relatively modest,[17,18] with the result that it is difficult to assess the importance of autoionization in the data.

Catani *et al.* have used photofragment spectroscopy to explore the electronic spectroscopy of the $C_4H_5^+$ cation.[19] They observed an electronic transition to a $^1A'$ state at ~4.68 eV above the ground state, and noted that this state maps directly onto the analogous excited state of the propargyl cation.[20,21] This excited state is well outside the range of energy of the present study. Catani *et al.* also performed electronic structure calculations of the $C_4H_5^+$ ground state and excited states, as well as for transitions between these states of $C_4H_5^+$ and their fragmentation processes. Several groups have performed additional electronic structure calculations on the electronic states of $C_3H_3^+$ and $C_4H_5^+$.[22-25]

For the present work, the single isomer 2-butyn-1-yl ($CH_3C{\equiv}C\text{-}{\bullet}CH_2$) radical (see Figure 1) was produced by H atom abstraction from 2-butyne by F atoms,[15] and the imaging photoelectron-photoion coincidence technique was used to reinvestigate the spectroscopy and dynamics of the radical. The combination of high photon flux and resolution of the DESIRS beamline[26] and associated instrumentation[27,28] at the SOLEIL Synchrotron allows photoelectron and photoion spectra to be recorded with a considerably improved combination of resolution and signal-to-noise ratio as compared to those measured previously. The goals for our study are to: (1) record the photoionization spectrum of the C_4H_5 butynyl radical at substantially higher resolution than previously reported to characterize electronically autoionizing resonances; (2) record high resolution TPES for both the electronic ground state and excited states of the cation; (3) determine if the near-threshold shape resonance observed in 2-butyne[29] is also present in the C_4H_5 radical; and (4) to determine the absolute photoionization cross section of C_4H_5. The coincidence approach applied here allows the simultaneous recording of the photoionization spectra for C_4H_4 and C_4H_3 produced by sequential H-atom abstraction reactions. The results on the C_4H_3 and C_4H_4 species will be discussed in a future publication.

II. EXPERIMENT

The experiments were performed at the DESIRS beamline of the Synchrotron SOLEIL, using the DELICIOUS III double-imaging photoelectron-photoion coincidence spectrometer.[26-28] As discussed previously, the target radicals were produced in a flow tube reactor by hydrogen abstraction from a suitable precursor (in this case 2-butyne entrained in He) by F atoms produced in a microwave discharge.[15,30] The 2-butyne (ABCR GmbH & Co., 98-99% purity) is a high-vapor pressure liquid at room temperature, and the gas above the liquid was used. For most of the experiments, the conditions were optimized for a single H abstraction. The beam of gas emerging from the flow tube passed through two skimmers before reaching the interaction region of the coincidence spectrometer, where it crossed the synchrotron beam. The DC extraction field used to collect the photoions and photoelectrons was 70.7 V/cm for photon energies between 7.7 and 9.5 eV, and 132.5 V/cm for energies between 9.4 and 11.0 eV. Any changes in the resulting transmission function were addressed by matching the intensities of the two data sets in the overlapping region between 9.4 and 9.5 eV. The observed ionization thresholds are expected to be shifted to lower energy by these electric fields by 6 meV (70.7 V/cm) and 9 meV (132.5 V/cm). These shifts correspond to 51 cm^{-1} and 70 cm^{-1}, respectively, or approximately one step in the spectra reported below.

The coincidence spectra were recorded by monitoring the signal as the photon energy was scanned across the range of interest. The photon energy was calibrated by using the third harmonic of the photon source and the ionization energy of He (24.5873 eV).[31] This calibration is accurate to approximately 3 meV for the ion yield scans from threshold to 9.5 eV, and 6 meV from 9.5 to 11.0 eV. A harmonics gas filter with Kr was used for these experiments, and the He calibration is confirmed by the position of two Kr absorption features at 10.0324 and 10.6437 eV.[31] For the measurements in which the monochromator was set to a particular energy (*i.e.*, the fixed energy photoelectron spectra and the absolute cross section measurement), the absolute photon energy is expected to be accurate to 10 meV. The photoelectron-photoion coincidence data were processed

to yield the wavelength scans as well as the Threshold or Slow Photo-Electron Spectra (TPES or SPES, respectively) of the C_4H_5 mass produced in the reactor. The latter can be separated from the residual background gas by the coincident ion image, which shows an identifiable supersonic region from the reactor species due to the adiabatic expansion through the first skimmer.[30] The images used to generate the signal were typically binned by a factor of two before processing. For the SPES data above 9.5 eV, however, this binning was increased to a factor of 8 to improve the signal to noise (S/N) ratio. As described previously,[15,32] the SPES data were obtained by integrating the photoelectron signal along lines of constant binding energy for a range of kinetic energies between 0 and a selected maximum energy, KE_{max}, which is chosen as a compromise between S/N ratio and resolution. Unless otherwise stated, the value of KE_{max} was 50 meV, which results in an effective resolution of 17 meV.[15,32] The overall uncertainties in the threshold determinations discussed below come from a combination of uncertainties in the photon energy and rotational envelope of the ionizing transition, and from the signal-to-noise ratio of the data.

Secondary reactions in the flow tube can produce macroscopic products that ultimately clog the first of the two skimmers. While an effort was made to minimize these reactions, the signal level dropped over the course of the long scans between 7.7 and 11.0 eV. To correct for this issue, fast scans were recorded across this energy range to obtain the correct overall shape of the spectrum. The relative intensities in the fast and long scans were then fit to provide a correction function for the latter scans. The spectra were also corrected for the variation in photon intensity and photodiode efficiency across the energy range of the spectrum. These two corrections introduce some uncertainty into the intensity of the photoion yield curve, particularly in the higher energy half of the spectrum (above 9.5 eV).

Preliminary experiments were also performed by selecting fixed photon energies and averaging the signal for considerably longer times (typically one hour) and reconstructing the data by using the pBASEX algorithm[33] to give both the photoelectron energy distribution and photoelectron-

energy-dependent angular distributions at these energies.

Geometry optimization and harmonic frequency calculations used in the determination of the Franck-Condon factors for photoionization to the $\tilde{X}^+ {}^1A'$ and $\tilde{a}^+ {}^3A''$ states of $C_4H_5^+$ were carried out at DFT level (M06-2X) using the aug-cc-pVTZ basis set using the Gaussian09 software package.[34] The Franck-Condon factors were then calculated using the harmonic approximation for vibrational frequencies and the normal modes in the neutral and cationic ground states, and assuming the transition dipole moment is independent of the vibrational coordinates (Condon approximation). The Duschinsky effect was considered using recursive formulae as implemented in Gaussian09.

III. RESULTS AND DISCUSSION

While there are a number of potential isomers of C_4H_5,[17,18] H atom abstraction from 2-butyne should preferentially result in the formation of the 2-butyn-1-yl ($CH_3C{\equiv}C\text{-}{\bullet}CH_2$) radical. The relevant thermochemistry and ionization energies for the C_4H_5 species are given in Table 1.[16,17,31,35] In what follows, we first present the SPES of the 2-butyn-1-yl radical, which provides information on the energetics of the electronic states of $C_4H_5^+$, followed by a discussion of the photoionization spectrum and the absolute photoionization cross section of C_4H_5. We conclude with a discussion of how the work can be complemented by fixed-energy photoelectron spectroscopy, and extended through the study of other isomers of the C_4H_5 radical.

A. The Slow Photoelectron Spectrum of C_4H_5

Figure 2 shows an overview SPES of C_4H_5 between the first ionization threshold and 11 eV. The spectrum shows three clear sets of bands near 7.9 eV, 9.7 eV, and 10.6 eV, corresponding to transitions from the neutral ground state $\tilde{X}\,{}^2A''$ to three different electronic states of the cation. The relative intensity of the first band is much greater than the intensities of the next two bands. This observation may be due to the influence of autoionization on the intensity of the origin band.

Expanded plots of the first two band systems are shown in Figures 3a and b. Additional weak structure is observed in scans between 11.3 and 11.5 eV, but the S/N ratio is too small to allow a meaningful characterization. Note that the dissociative ionization threshold to produce the 2-butyn-1-yl cation from 2-butyne is ~11.98 eV,[31] outside the range of the current experiments.

The TPES for the first band of the 2-butynyl radical has been reported previously by Lang *et al*.,[16] and corresponds to the transition to the $\tilde{X}^+$ $^1A'$ ground state of $C_4H_5^+$. The present SPES is in excellent agreement with the TPES, and shows somewhat better resolved vibrational structure. Corrected for the Stark shift, our ionization threshold of 7.93 ± 0.01 eV is also in excellent agreement with the value of 7.94 ± 0.02 eV from Lang *et al*.[16] The instrumental resolution for the TPES of Lang *et al.* (5 meV)[16] is actually higher than that of the present SPES spectrum, although the S/N of the present spectrum is better. Interestingly, the features in the present SPES are better resolved that in the TPES of Lang *et al.*, perhaps suggesting a higher rotational temperature in the pyrolysis source used in the earlier experiments. The SPES shows several additional peaks corresponding to vibrational bands of the $\tilde{X}^+$ $^1A'$ state of $C_4H_5^+$. As indicated in Figure 3a, these features fall into two short progressions, for which we use the numbering scheme of Catani *et al*.,[19] with the energies given in Table 2. Theoretical calculations performed by Lang *et al*.[16] indicate that these correspond to excitation of ν_{11}^+ (stretch of the two C-C single bonds) at 806 cm^{-1} (0.100 eV), and excitation of ν_4^+ (stretch of the C≡C triple bond) at 2243 cm^{-1} (0.278 eV). The agreement with the predicted values of the vibrational frequencies is quite good. Figure 3a shows a Franck-Condon simulation of the $\tilde{X}^+$ $^1A'$ band system that was calculated using the Gaussian electronic structure codes and density functional theory with M06-2X aug-cc-pVTZ functionals. The ionization energy calculated at this level is somewhat below the more accurate calculations reported by Hansen *et al*.,[17] and the present results have been shifted to agree with the experimental ionization energy. The calculated spectrum has also been convoluted with a 30 meV FWHM Gaussian function to account for the experimental resolution and for the rotational contour, and the overall intensity has been scaled to match the experimental intensity of the origin band. As

seen in Figure 3a, the agreement with the experiment is good, but the intensity of the vibrationally excited peaks in the experimental progressions falls off faster than in the simulation. Some weaker features associated with several other vibrational modes are present in the simulation, but the corresponding features are not obvious in the experimental spectrum.

Neither the TPES nor SPES of the excited electronic states of $C_4H_5^+$ has been reported previously, although Hansen *et al.*[17] provided a theoretical value for the first excited state threshold, corresponding to the $\tilde{a}^+$ ^{3}A" state with an ionization energy of 9.74 eV (see Table 1). Figure 3b shows a single progression with an origin at 9.74 ± 0.02 eV, in excellent agreement with the predicted position for the $\tilde{a}^+$ state. The band positions, vibrational energies, and proposed assignments are reported in Table 2. Figure 3b also shows a Franck-Condon simulation for the transition to the $\tilde{a}^+$ ^{3}A" state calculated in the same manner as that for the $\tilde{X}^+$ ^{1}A' state. Both the experiment and simulation show a strong progression in the ν_4^+ C≡C stretch, but the experimental vibrational energies are somewhat smaller than the theoretical values. This observation maybe be at least partially due to the neglect of anharmonicity in the calculated spectrum. Nevertheless, the experimental and vibrational intensities within the vibrational progression are in good agreement. Both the experimental and theoretical spectra show weaker structure between the members of the ν_4^+ progression, but the signal to noise ratio in the experiment is insufficient to characterize this in any detail. Nevertheless, as seen in Figures 3a and b, our calculations predict that one should also observe the ν_{11}^+ vibrational mode in the transition towards the ground state of the cation and several weak combination bands involving the ν_8^+, ν_{10}^+, ν_{18}^+, and ν_{21}^+ modes in the transition towards the $\tilde{a}^+$ state.

The third SPES band for C_4H_5 observed in Figure 2 most likely results from the transition to the $\tilde{A}^+$ ^{1}A" state of the 2-butyn-1-yl $C_4H_5^+$ cation. The signal-to-noise ratio in this part of the spectrum is relatively low. The single strong feature in this region yields a value of 10.626 ± 0.030 eV for the $\tilde{A}^+$ ^{1}A" ionization energy (see Table 1). No theoretical ionization energy or vibrational

frequencies have been reported for this state previously. The energy of this state was calculated by using Electron Propagator Theory (EPT) as implemented in the Gaussian software suite,[34] and the calculation puts this state approximately 0.6 eV above the $\tilde{a}^+ {}^3A''$ state, consistent with previous calculations.[36-38] Using our experimental ionization energy for the latter state yields a predicted $\tilde{A}^+ {}^1A''$ ionization energy of ~10.34 eV, somewhat lower than the present experimental value. Improvements in the S/N ratio in this region of the SPES would allow a better characterization of this state. However, comparison with the electronic structure of the propargyl cation[15] provides support for this assignment. In particular, the $\tilde{a}^+ {}^3A_2$ and $\tilde{A}'^+ {}^1A_2$ states of $C_3H_3^+$ lie 1.809 and 2.683 eV above the $\tilde{X}^+ {}^1A_1$ ground state, respectively,[15,39] while the present $\tilde{a}^+ {}^3A''$ and $\tilde{A}^+ {}^1A''$ states of $C_4H_5^+$ lie 1.81 and 2.70 eV above the corresponding $\tilde{X}^+ {}^1A'$ ground state. The first excited $^1A_1$ states of $C_3H_3^+$ and $CH_3CCCH_2^+$ also lie at similar energies above the corresponding ground state cations. Systematic quantum chemical studies of the similarities of these systems, and related systems such as $CHBrCCH^+$, should prove informative.[40]

B. The Photoionization Spectrum of C_4H_5

Figure 4 shows a plot of the $C_4H_5^+$ photoionization cross section between 7.7 and 11.0 eV. This cross section has been put on an absolute scale using the value of the cross section determined at 9.7 eV, as described in Section III.C. While we are confident about the overall shape of the spectrum, the uncertainty in the total intensity at the peak of the broad feature near 10.5 eV may be as large as 25 - 35% due to uncertainties discussed in the experimental section. The spectrum shows a sharp rise at threshold with significant resonant structure up to about 9.5 eV, followed by a second, more gradual rise up to approximately 10.5 eV, then gradually falling to still higher energy. This second rise also shows a second set of resonant structure that appears to converge to a limit near 10.6 eV.

As in the case of the propargyl radical,[13-15] the intense features within the first 0.5 eV of the ionization threshold almost certainly correspond to electronically autoionizing Rydberg states

based on excited states of the cation. A combination of factors makes it unlikely that resolved Rydberg states will be observed converging to vibrationally excited levels of the $\tilde{X}^+ {}^1A'$ ground state between 7.93 and 8.47 eV. In particular, because the relevant vibrational thresholds are only a few tenths of an eV above the observed onset, the principal quantum numbers of Rydberg states above this onset and converging to these vibrational thresholds are relatively high, with correspondingly small spacings between adjacent series members. In addition, the Franck-Condon factors to these excited vibrational levels, and thus to the Rydberg series converging to them, are small. Finally, the intense electronic autoionization features will tend to swamp the transitions converging to vibrationally excited thresholds of the $\tilde{X}^+ {}^1A'$ state.

Figure 4 shows distinct similarities to the spectrum of the propargyl radical.[13-15] Indeed, the latter spectrum displays intense resonance structure that appears to converge to the analogous excited electronic states of the cation. This similarity between the propargyl and 2-butyn-1-yl spectra reflects the similarity of the two singly occupied radical orbitals of these species, which have "dπ" character perpendicular to the plane of the CH_2 group. As in the propargyl cation spectrum, neither region of resonance structure in the C_4H_5 photoionization spectrum shows obvious signs of regularity. Assuming the observed structure corresponds to series converging to either the $\tilde{a}^+ {}^3A''$ or $\tilde{A}^+ {}^1A''$ states of the cation, the quantum defects, δ, can be calculated by using:

$$n^* = n - \delta = \sqrt{\frac{\mathcal{R}}{IE - E}} \quad , \qquad (2)$$

where n^* is the effective principal quantum number, $\mathcal{R}$ is the mass-corrected Rydberg constant[41] for C_4H_5 (13.60555 eV), IE is the ionization energy, and E is the resonance energy. Either the adiabatic ionization thresholds or the vibrationally excited thresholds (see Tables 1 and 2) can be used. This approach does not reveal any systematic regularity in the lower energy portion of the spectrum. This observation suggests that the structure in this region is perturbed, most likely through the interaction of series converging to the two ($\tilde{a}^+ {}^3A''$ and $\tilde{A}^+ {}^1A''$) excited state thresholds,

or through Rydberg/valence state mixing. At higher energy, however, a few members of a fairly regular series with a slowly increasing quantum defect can be identified converging to the $\tilde{A}^+ {}^1A''$ threshold at 10.626 eV. This series is indicated in Figure 4. If a slightly lower value of 10.614 eV is used for the ionization energy (corresponding to ~1 scanning step in the spectrum), the quantum defect for these features remains nearly constant at $\delta = 0.85$. Although the orbital angular momentum of the Rydberg electron, *l*, is not expected to be a good quantum number in a molecule, such a value of δ is typically associated with an "*n*s" Rydberg series. Ionization of the 2-butyn-1-yl radical to the $\tilde{A}^+ {}^1A''$ state corresponds to the removal of an electron from an "ungerade" orbital in the π system, and as a result, excitation to an "*n*s" Rydberg series is not surprising.

A more detailed analysis of the electronic autoionization structure will require more extensive theoretical calculations of the excited states of the 2-butyn-1-yl radical and cation. As in earlier studies of propyne[42] and 2-butyne,[43] the calculation of the partial photoionization cross sections to the $\tilde{X}^+ {}^1A'$, $\tilde{a}^+ {}^3A''$, and $\tilde{A}^+ {}^1A''$ states, and more specifically the partial wave decompositions of those cross sections, could provide insight into which Rydberg series are expected to dominate to each ionization threshold. Such calculations may also serve to reveal which channels, and thus which Rydberg series, interact most strongly. It is also possible that such calculations will reveal shape resonances in photoionization from the singly occupied molecular orbital (SOMO). For 2-butyne, the photoionization cross section shows a very intense maximum just above threshold that corresponds to a shape resonance.[43,44] Although there appears to be a broad maximum centered at about ~10.5 eV in the 2-butyn-1-yl spectrum of Figure 4, it is nowhere nearly as dramatic as in the 2-butyne spectrum. Given the dominant "dπ" character of the SOMO, shape resonances with "fσ" and "fπ" character may be most relevant for the 2-butyn-1-yl radical.

C. The Absolute Photoionization Cross Section of C_4H_5

The absolute photoionization cross section of the C_4H_5 radical was determined at a photon energy of 9.7 eV by using a variation of methods described previously for CH_3 and C_2H_5.[45,46] The photon

energy was chosen to be just above the ionization threshold of the precursor 2-butyne molecule. In particular, the 2-butyne precursor (mass 54) and 2-butynyl fragment (mass 53) ion signals were monitored as a function of the length of the interaction region with F atoms in the flow tube. Conditions were chosen to minimize secondary chemistry. The relative ion signals at the two masses were measured over a range of conditions in which sequential abstractions and F and F_2 addition reactions were minimized. The mass spectrum was measured with the microwave discharge off (no F and hence no C_4H_5 production) and on, and the decrease in the $C_4H_6^+$ signal ($\Delta S(C_4H_6^+)$) was compared with the increase in $C_4H_5^+$ signal ($\Delta S(C_4H_5^+)$) to determine the cross section ratio. The depletion of the $C_4H_6^+$ signal when the discharge was on ranged from 18 to 27%. The main advantage of this method is that since the species differ by only one mass unit, the difference in their mass discrimination factors is negligible and no calibration of the spectrometer is required. A small signal was observed at mass 52 ($C_4H_4^+$) that changed only a small amount with the discharge on. The known absolute photoionization cross section of 2-butyne[47] at 9.7 eV (44.9 ± 9.0 Mb) was then used to yield the absolute photoionization cross section of the 2-butynyl radical using:

$$\sigma_{ion}(C_4H_5) = \sigma_{ion}(C_4H_6)\left(\frac{\Delta S(C_4H_5^+)}{\Delta S(C_4H_6^+)}\right) \quad . \qquad (3)$$

Averaging the results of eighteen separate measurements gave an average absolute cross section for C_4H_5 at 9.7 eV of 6.1 ± 1.8 Mb, with a 2σ confidence interval. This value was used to provide an absolute scale for the C_4H_5 photoionization yield in Figure 4.

Recently, the absolute photoionization cross-section of 2-butyn-1-yl has been calculated by Huang et al.,[48] using a method previously outlined by Moshammer et al.[49] This method involves calculating the transition moment, *D*, with a single channel frozen-core Hartree−Fock method, and calculating the Franck-Condon overlap envelope, *S*, within the harmonic approximation. In this

approach, the resulting cross section is given by $\sigma(E) = D(E)S(E)$. This method has been benchmarked against various species, and the authors reported an agreement of better than a factor of 2 for the absolute cross-sections. However, even though the contributions of autoionizing resonances are not considered in their calculations, the photoionization curve for 2-butyn-1-yl of Huang et al. shows values of up to ~36 Mb at 8.2 eV, in stark disagreement with our low (~5Mb) values at this photon energy.

IV. CONCLUSION

The flow tube source using fluorine atoms to abstract H atoms from hydrocarbon precursors is once again shown to be an effective source for photoionization studies of radicals. We have presented new data on the photoionization of the 2-butyn-1-yl C_4H_5 radical. The SPES of C_4H_5 presented here provides an improved determination of the adiabatic ionization energy and some vibrational frequencies of the $\tilde{X}^+\ ^1A'$ state of the cation. This SPES also provides the first experimental determination of the energetics of the $\tilde{a}^+\ ^3A''$ and $\tilde{A}^+\ ^1A''$ excited electronic states of the cation. As expected, the spacings between the $\tilde{X}^+\ ^1A'$, $\tilde{a}^+\ ^3A''$, and $\tilde{A}^+\ ^1A''$ states of $CH_3C{\equiv}CCH_2^+$ are very similar to those between the $\tilde{X}^+\ ^1A_1$, $\tilde{a}^+\ ^3A_2$, and $\tilde{b}^+\ ^1A_2$ states of the $HC{\equiv}CCH_2^+$ propargyl cation.[15]

The present photoionization spectra of the C_4H_5 radical is of considerably higher resolution and *S/N* ratio than the previously reported spectra. The spectrum shows resonance structure that corresponds to transitions to electronically autoionizing states converging to excited electronic state of the cations. This structure shows very little regularity, although one series is tentatively assigned as converging to the $\tilde{A}^+\ ^1A''$ state of $C_4H_5^+$. As expected, the C_4H_5 spectrum also shows distinct similarities to the photoionization spectrum of the propargyl radical, which displays strong resonance features associated with Rydberg series converging to excited states of the cation. To date, the assignments of these features in the propargyl and C_4H_5 spectra are tentative at best.[13-15] A systematic study of both radicals using high resolution photoelectron imaging as a function of

photon energy may allow the classification of different resonances based on the electronic and vibrational branching ratios, and on the photoelectron angular distributions following autoionization of the different resonances. Such photoelectron images would be particularly interesting above ~9.8 eV, where ionization can access vibrational levels of both the $\tilde{X}^+ {}^1A'$ and $\tilde{a}^+ {}^3A''$ states of $C_4H_5^+$. For resonances converging to the $\tilde{A}^+ {}^1A''$ state, the branching between these two final states will reveal the relative strength of the configuration interaction matrix elements driving the two electronic autoionization processes. Our preliminary spectra suggest that both branching fractions and angular distributions do show energy-dependent behavior. Recent improvements in the imaging lens system are expected to allow much more detailed studies of the decay dynamics in future work.

The methodology reported here to measure absolute ionization cross sections of radicals has the potential of being applicable to many hydrocarbon radicals provided that secondary abstraction reactions can be avoided or taken into account, as is the case for C_4H_5. These values are critical for quantitative detection in gas phase reactions, or to model other complex environments, where these species might be present and play a role in the chemistry. The comparison to computed absolute cross sections highlights the difficulty of the calculations and experiments, and the necessity of continuing both experimental and theoretical efforts to take full advantage of these advanced mass-spectrometry techniques for species determination.

Analogous studies of the C_4H_5 radicals formed from other precursors should also prove interesting, and allow us to determine if the observation of strong resonance structure is somehow connected to the relative stability of the propargyl cation. In particular, studies using 1-butyne and 1,2-butadiene as precursors will allow the study of multiple additional isomers in which the H atoms are not all confined to the terminal carbon atoms. The double-imaging, photoelectron-photoion coincidence technique should allow the separation of contributions from the different isomers, and provide new insight into the electronic structure of these fundamental hydrocarbon radicals

ACKNOWLEDGEMENTS

DMPH was supported by the Science and Technology Facilities Council, UK. This material is based on work supported by the U.S. Department of Energy, Office of Science, Office of Basic Energy Sciences, Division of Chemical Sciences, Geosciences, and Biosciences respectively under contract No. DE-AC02-06CH11357 (STP). This work has received financial support from the French Agence Nationale de la Recherche (ANR) under Grant No. ANR-12-BS08-0020-02 (project SYNCHROKIN). The experiments were performed on the DESIRS Beamline at SOLEIL under proposal number 20160857. We are grateful to the entire staff of SOLEIL for running the facility.

REFERENCES

1. Klippenstein, S. J. From theoretical reaction dynamics to chemical modeling of combustion, *Proc. Comb. Inst.* **2017**, *36*, 77-111.
2. Law, C. K. *Combustion Physics* (Cambridge University, New York, 2006).
3. Alman, D. A.; Ruzic, D. N.; Brooks, J. N. A hydrocarbon reaction model for low temperature hydrogen plasmas and an application to the Joint European Torus, *Phy. Plasmas* **2000**, *7*, 1421-1432.
4. Wayne, R. P. *Chemistry of Atmospheres* (Oxford University, New York, 2002).
5. Taatjes, C. A.; Hansen, N.; McIlroy, A.; Miller, J. A.; Senosiain, J. P.; Klippenstein, S. J.; Qi, F; Sheng, L. S.; Zhang, Y. W.; Cool, T. A.; et al. Enols are common intermediates in hydrocarbon oxidation, *Science* **2005**, *308*, 1887-1889.
6. Taatjes, C. A.; Hansen, N.; Osborn, D. L.; Kohse-Höinghaus, K.; Cool, T. A.; Westmoreland, P. R.; Imaging combustion chemistry via multiplexed synchrotron photoionization mass spectrometry, *Phys. Chem. Chem. Phys.* **2008,** *10*, 20-34.
7. Hansen, N.; Cool, T. A.; Westmoreland, P. R.; Kohse-Hoinghaus, K. Recent contributions of flame-sampling molecular-beam mass spectrometry to a fundamental understanding of combustion chemistry. *Prog. Energy Comb. Sci.* **2009**, *35*, 168-191.
8. Cool, T. A.; Nakajima, K.; Mostefaoui, T. A.; Qi, F.; McIlroy, A.; Westmoreland, P. R.; Law, M. E.; Poisson, L.; Peterka, D. S.; and Ahmed, M. Selective detection of isomers with photoionization mass spectrometry for studies of hydrocarbon flame chemistry, *J. Chem. Phys.* **2003**, *119*, 8356-8365.
9. Taatjes, C. A. Uncovering the fundamental chemistry of alkyl + O_2 reactions via measurements of product formation, *J. Phys. Chem. A* **2006**, *110*, 4299-4312.
10. Berkowitz, J. *Atomic and Molecular Photoabsorption: Absolute Partial Cross Sections* (Academic, Cambridge, 2015).
11. Berkowitz, J. *Photoabsorption, Photoionization, and Photoelectron Spectroscopy* (Academic, New York, 1979)

12. Pratt, S. T. High-resolution valence-shell photoionization, in *Handbook of High-Resolution Spectroscopy*, edited by M. Quack and F. Merkt, (Wiley, West Sussex, UK, 2011), Vol. 3, p. 1595-1616.

13. Zhang, T.; Tang, X. N.; Lau, K. C.; Ng, C. Y.; Nicolas, C.; Peterka, D. S.; Ahmed, M.; Morton, M. L.; Ruscic, B.; Yang, R.; et al. Direct identification of propargyl radical in combustion flames by vacuum ultraviolet photoionization mass spectrometry, *J. Chem. Phys.* **2006**, *124*, 074302.

14. Savee, J. D.; Soorkia, S.; Welz, O.; Selby, T. M.; Taatjes, C. A.; Osborn, D. L. Absolute photoionization cross-section of the propargyl radical, *J. Chem. Phys*. **2012**, *136*, 134307.

15. Garcia, G. A.; Gans, B.; Krüger, J.; Holzmeier, F.; Röder, A.; Lopes, A.; Fittschen, C.; Alcaraz, C.; Loison, J. C. Valence shell threshold photoelectron spectroscopy of C_3H_x (x = 0-3), *Phys. Chem. Chem. Phys.*, **2018**, *20*, 8707- 8718.

16. Lang, M.; Holzmeier, F.; Hemberger, P.; Fischer, I. Threshold photoelectron spectra of combustion relevant C_4H_5 and C_4H_7 isomers, *J. Phys. Chem. A* **2015**, *119*, 3995-4000.

17. Hansen, N.; Klippenstein, S. J.; Taatjes, C. A.; Miller, J. A.; Wang, J.; Cool, T. A.; Yang, B.; Yang, R.; Wei, L.; Huang, C.; et al. Identification and chemistry of C_4H_3 and C_4H_5 isomers in fuel-rich flames, *J. Phys. Chem. A* **2006**, *110*, 3670-3678.

18. Chin, C. H.; Chen, W. K.; Huang, W. J.; Lin, Y. C.; Lee, S. H. Identification of C_4H_5, C_4H_4, C_3H_3, and CH_3 radicals produced from the reaction of atomic carbon with propene: Implications for the atmospheres of Titan and giant planets and for the interstellar medium, *Icarus*, **2013**, *222*, 254-262.

19. Catani, K. J.; Muller, G.; da Silva, G.; Bieske, E. J. Electronic spectrum and photodissociation chemistry of the linear methyl propargyl cation $H_2C_4H_3^+$, *J. Chem. Phys.* **2017**, *146*, 044307.

20. Catani, K. J.; Sanelli, J. A.; Dryza, V.; Gilka, N.; Taylor, P. R.; Bieske, E. J. Electronic spectrum of the propargyl cation ($H_2C_3H^+$) tagged with Ne and N_2, *J. Chem. Phys.* **2015**, *143*, 184306.

21. Wyss, M.; Riaplov, E., Maier, J. P. Electronic and infrared spectra of $H_2C_3H^+$ and cyclic $C_3H_3^+$ in neon matrices, *J. Chem. Phys.* **2001**, *114*, 10355-10361.

22. Botschwina, P.; Oswald, R. Calculated photoelectron spectra of isotopomers of the propargyl radical (H_2C_3H): an explicitly correlated coupled cluster study, *Chem. Phys.* **2010**, *378*, 4-10.

23. Botschwina, P.; Oswald, R.; Rauhut, G. Explicitly correlated coupled cluster calculations for the propargyl cation($H_2C_3H^+$) and related species, *Phys. Chem. Chem. Phys.* **2011**, *13*, 7921-7929.

24. Douberly, G. E.; Ricks, A. M.; Ticknor, B. W.; McKee, W. C.; Schleyer, P. v. R.; Duncan, M. A. Infrared photodissociation spectroscopy of protonated acetylene and its clusters, *J. Phys. Chem. A* **2008**, *112*, 1897-1906.

25. Cunje, A.; Rodriguez, C. F.; Lien, M. H.; Hopkinson, A. C. The $C_4H_5^+$ potential energy surface. Structure, relative energies, and enthalpies of formation of isomers of $C_4H_5^+$, J. *Org. Chem.* **1996**, *61*, 5212-5220.

26. Nahon, L.; de Oliveira, N.; Garcia, G. A.; Gil, J. F.; Pilette, B.; Marcouillé, O.; Lagarde, B.; Polack, F. DESIRS: a state-of-the-art VUV beamline featuring high resolution and variable polarization for spectroscopy and dichroism at SOLEIL, *J. Synchrotron Radiat.* **2012**, *19*, 508-520.

27. Garcia, G. A.; Cunha de Miranda, B. K.; Tia, M.; Daly, S.; Nahon, L. DELICIOUS III: a multipurpose double imaging particle coincidence spectrometer for gas phase vacuum ultraviolet photodynamics studies, *Rev. Sci. Instrum*. **2013**, *84*, 053112.

28. Tang, X.; Garcia, G. A.; Gil, J.-F.; Nahon, L. Vacuum upgrade and enhanced performances of the double imaging electron/ion coincidence end-station at the vacuum ultraviolet beamline DESIRS, *Rev. Sci. Instrum*. **2015**, *86*, 123108.

29. Xu, H.; Jacovella, U.; Ruscic, B.; Pratt, S. T.; Lucchese, R. R. Near-Threshold Shape Resonance in the Photoionization of 2-Butyne. *J. Chem. Phys.* **2012**, *136*, 154303.

30. Garcia, G. A.; Tang, X.; Gil, J. F.; Nahon, L.; Ward, M.; Batut, S.; Fittschen, C.;

Taatjes, C. A.; Osborn, D. L.; Loison, J. C. Synchrotron-based double imaging photoelectron/photoion coincidence spectroscopy of radicals produced in a flow tube: OH and OD. J. Chem. Phys. **2015**, ***142***, 164201.

31. NIST Chemistry WebBook at http://webbook.nist.gov, July 1, 2015.
32. Poully, J. C.; Schermann, J. P.; Nieuwjaer, N.; Lecomte, F.; Gregoire, G.; Desfrancois, C.; Garcia, G. A.; Nahon, L.; Nandi, D.; Poisson, L.; et al. Photoionization of 2-pyridone and 2-hydroxypyridine, *Phys. Chem. Chem. Phys.* **2010**, *12*, 3566-3572.
33. Garcia, G. A.; Nahon, L.; Powis, I. Two-dimensional charged particle image inversion using a polar basis function expansion, *Rev. Sci. Instrum*. **2004**, *75*, 4989-4996
34. Frisch, M. J.; Trucks, G. W.; Schlegel, H. B.; Scuseria, G. E.; Robb, M. A.; Cheeseman, J. R.; Scalmani, G.; Barone, V.; Mennucci, B.; Petersson, G. A.; et al. Gaussian 09, Gaussian, Inc., Wallingford CT, 2009.
35. Wheeler, S. E.; Allen, W. D.; Schaefer, H. F. Thermochemistry of disputed soot formation intermediates C_4H_3 and C_4H_5, *J. Chem. Phys*. **2004**, *121*, 8800-8813.
36. Eyler, J. R.; Oddershede, J.; Sabin, J. R.; Diercksen, G. H. F.; Grüner, N. E., Excitation energy of linear $C_3H_3^+$. Can this ion be detected by laser-induced fluorescence in flames?, *J. Phys. Chem.* **1984**, *88*, 3121-3123.
37. Takada, T.; Ohno, K., *Ab initio* LCAO MO SCF CI Calculations on the electronic structure of the cyclopropenyl cation. *Bull. Chem. Soc. Japan* **1979**, *52*, 334-338.
38. Cameron, A.; Leszczynski, J; Zerner, M. C.; and Weiner, B., Structure and properties of $C_3H_3^+$ cations, *J. Phys. Chem.* **1989**, *93*, 139-144.
39. The lowest singlet excited state of CH_2CCH^+ has $^1A_2$ symmetry, and would traditionally have been labeled A $^1A_2$. However, in References 20 and 21, the first allowed electronic transition from the X $^1A_1$ state of CH_2CCH^+ to a higher energy $^1A_1$ state was labeled A $^1A_1$ ← X $^1A_1$. In Reference 15, the present $^1A_2$ state was labeled b $^1A_2$. Because singlet states are traditionally labeled with capital letters, here we have relabeled this state A' $^1A_2$.

40. Hemberger, P.; Lang, M.; Noller, B.; Fischer, I.; Alcaraz, C.; Cunha de Miranda, B. K.; Garcia, G. A.; Soldi-Lose, H., Photoionization of propargyl and bromopropargyl radicals: A threshold photoelectron spectroscopic study. *J. Phys. Chem. A* **2011**, *115*, 225-2230.

41. Shore, B. W.; Menzel, D. H. *Principles of Atomic Spectra* (Wiley, New York, 1968).

42. Jacovella, U.; Holland, D. M. P.; Boyé-Péronne, S.; Joyeux, D.; Archer, L. E.; de Oliveira, N.; Nahon, L.; Lucchese, R. R.; Xu, H.; Pratt, S. T. High-resolution photoabsorption spectrum of jet-cooled propyne. *J. Chem. Phys*. **2014**, *141*, 114303.

43. Jacovella, U.; Holland, D. M. P.; Boyé-Péronne, S.; Gans, B.; de Oliveira, N.; Joyeux, D.; Archer, L. E.; Lucchese, R. R.; Xu, H.; Pratt, S. T., High-resolution vacuum-ultraviolet photoabsorption spectra of 1-butyne and 2-butyne. *J. Chem. Phys*. **2015**, *143*, 034304.

44. Jacovella, U.; Holland, D. M. P.; Boyé-Péronne, S.; Gans, B.; de Oliveira, N.; Ito, K.; Joyeux, D.; Archer, L. E.; Lucchese, R. R.; Xu, H.; et al. A near-threshold shape resonance in the valence shell photoabsorption of linear alkynes, *J. Phys. Chem. A.* **2015**, *119*, 12339-12348.

45. Loison, J. C., Absolute photoionization cross section of the methyl radical, *J. Phys. Chem. A* **2010**, *114*, 6515-6520.

46. Gans, B.; Garcia, G. A.; Boyé-Péronne, S.; Loison, J. C.; Douin, S.; Gaie-Levrel, F.; Gauyacq, D., Absolute photoionization cross section of the ethyl radical in the range 8-11.5 eV: synchrotron and vacuum ultraviolet laser measurements, *J. Phys. Chem. A* **2011**, *115*, 5387-5396.

47. Wang, J.; Yang, B.; Cool, T. A.; Hansen, N.; Kasper, T., Near-threshold absolute photoionization cross sections of some reaction intermediates in combustion. *Int. J. Mass Spectrom.* **2008**, *269*, 210-220.

48. C. Huang, B. Yang, F. Zhang, and G. Tian, Quantification of the resonance stabilized C_4H_5 isomers and their reaction with acetylene. *Combust. Flame* **2018**, *198*, 334-341.

49. Moshammer, K.; Jasper, A. W.; Popolan-Vaida, D. M.; Wang, Z.; Bhavani Shankar, V. S.; Ruwe, L.; Taatjes, C. A.; Dagaut, P.; Hansen, N., Quantification of the keto-hydroperoxide

(HOOCH$_2$OCHO) and other elusive intermediates during low-temperature oxidation of dimethyl ether. *J. Phys. Chem. A* **2016**, *120***,** 7890-7901.

Table 1. Thermochemistry and Ionization Energies of C_4H_5.

Species	Ionization energy (eV)				C_4H_5 Δ_fH^o (0K) (kJ/mol)
		$\tilde{X}^+ {}^1A'$	$\tilde{a}^+ {}^3A''$	$\tilde{A}^+ {}^1A''$	
C_4H_5 ($CH_3C{\equiv}C\text{-}{\bullet}CH_2$)	Exp. (this work)	7.930 ± 0.010	9.74 ± 0.02	10.63 ± 0.03	319.2
	Theory.[a]	7.94	9.74	-	
	Exp.[b]	7.94 ± 0.02	-	-	

a: from Hansen *et al*. (ref. 17)
b : from Lang *et al*. (ref. 16)

Table 2. Vibrational Energies for $C_4H_5^+$.

Ionic State	Vibrational Energy (cm^{-1})			Assignment
	This work	Previous work[a]	Theory[b]	
$\tilde{X}^+ {}^1A'$	0	0	0	origin
	787±30	806	789	11_0^1 C-C stretches
	1492±30	-	1577	11_0^2
	2153±50	2243	2200	4_0^1 C≡C stretch
	4308±50	-	-	4_0^2
$\tilde{a}^+ {}^3A''$	0	-	-	origin
	1637±30	-	1905	4_0^1 C≡C stretch
	3411±30	-	3809	4_0^2
$\tilde{A}^+ {}^1A''$	0	-	-	origin

a. From Hansen *et al*., reference 17.
b. Present calculations performed at the DFT level (M06-2X) using an aug-cc-pVTZ basis set .

FIGURE CAPTIONS

Figure 1. A schematic drawing of the structure of the propargyl radical and two isomers of the C_4H_5 radical.

Figure 2. The slow photoelectron spectrum (SPES) of C_4H_5 between 7.7 and 11.0 eV, with a resolution of 17 meV and the proposed assignment of the observed vibronic structures.

Figure 3. Expanded portions of the SPES of C_4H_5, along with a simulation based on Franck-Condon factors for the ionizing transition. (a) The $\tilde{X}^+ {}^1A'$ band. The simulation has been shifted to higher energy by 0.025 eV to match the energy of the experiment. (b) The $\tilde{a}^+ {}^3A''$ band. The simulation has been shifted to higher energy by 0.26 eV to match the energy of the experiment. The vibrational structure is discussed in the text.

Figure 4. The photoionization cross section of C_4H_5 between 7.7 and 11.0 eV obtained by detecting the $C_4H_5^+$ ion signal. The labeled resonances correspond to a Rydberg series with near constant quantum defect converging to the $\tilde{A}^+ {}^1A''$ state. The red circle and error bar indicates the result of the absolute cross section measurement at 9.7 eV. Asterisks indicate absorption lines of Kr present in the gas filter and responsible for a decrease in the VUV flux.

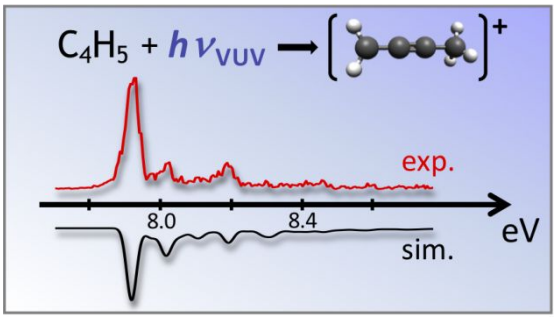

TOC Graphic

Figure 1

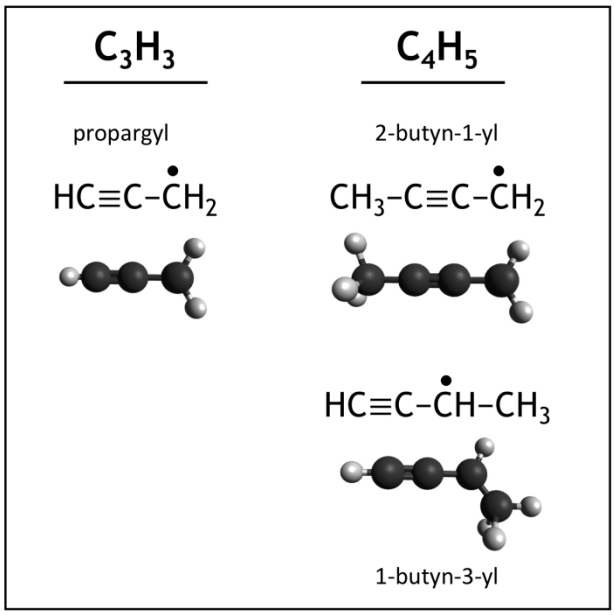

Figure 1. A schematic drawing of the structure of the propargyl radical and two isomers of the C_4H_5 radical.

296x209mm (200 x 200 DPI)

Figure 2

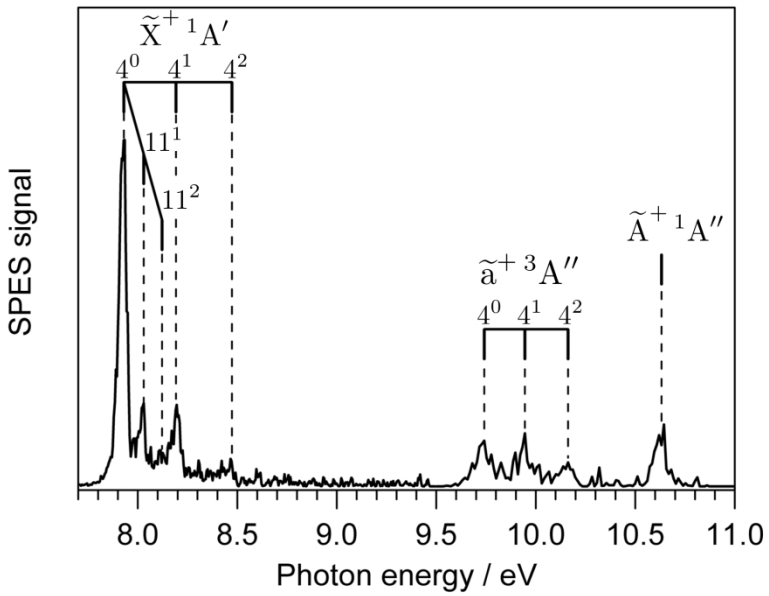

Figure 2. The slow photoelectron spectrum (SPES) of C_4H_5 between 7.7 and 11.0 eV, with a resolution of 17 meV and the proposed assignment of the observed vibronic structures.

296x209mm (200 x 200 DPI)

Figure 3

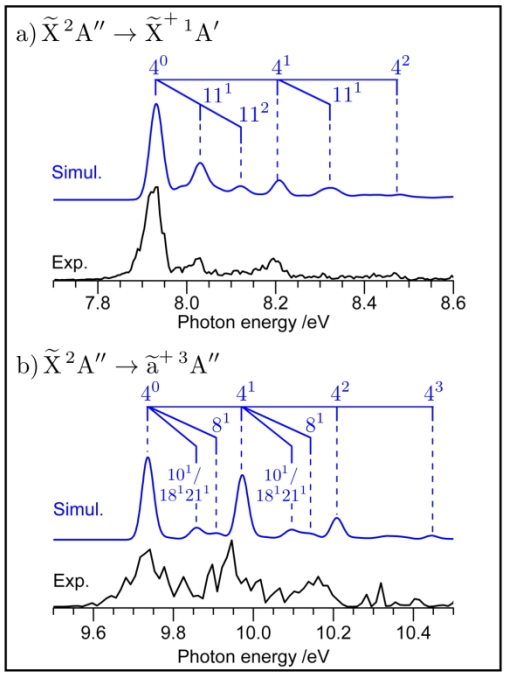

Figure 3. Expanded portions of the SPES of C_4H_5, along with a simulation based on Franck-Condon factors for the ionizing transition. (a) The $\tilde{X}^+$ $^1A'$ band. The simulation has been shifted to higher energy by 0.025 eV to match the energy of the experiment. (b) The $\tilde{a}^+$ $^3A''$ band. The simulation has been shifted to higher energy by 0.26 eV to match the energy of the experiment. The vibrational structure is discussed in the text.

296x209mm (200 x 200 DPI)

Figure 4

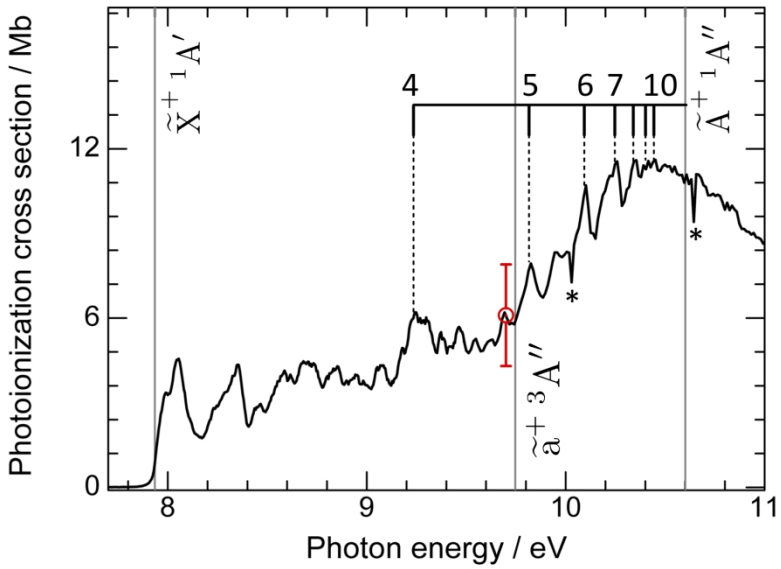

Figure 4. The photoionization cross section of C_4H_5 between 7.7 and 11.0 eV obtained by detecting the $C_4H_5^+$ ion signal. The labeled resonances correspond to a Rydberg series with near constant quantum defect converging to the A $^+$ ^{1}A" state. The red circle and error bar indicates the result of the absolute cross section measurement at 9.7 eV. Asterisks indicate absorption lines of Kr present in the gas filter and responsible for a decrease in the VUV flux.

296x209mm (200 x 200 DPI)

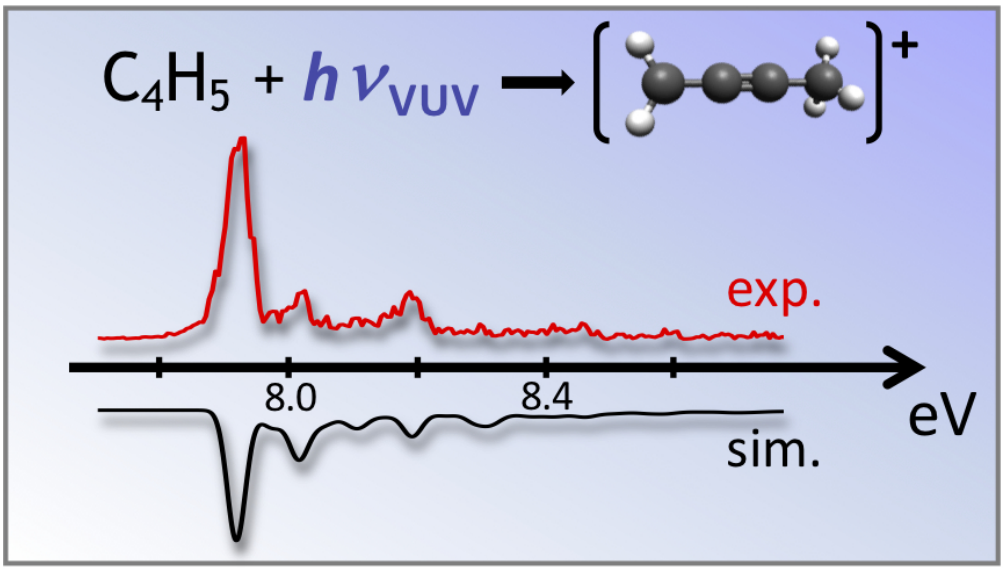

Table of Contents Graphic

72x41mm (300 x 300 DPI)